Eur. Phys. J. D (2016) 70: 237
DOI: 10.1140/epjd/e2016-70390-3

THE EUROPEAN PHYSICAL JOURNAL D

Colloquium

Evaluating experimental molecular physics studies of radiation damage in DNA*

Małgorzata A. Śmiałek[1,2,a]

[1] Department of Control and Power Engineering, Faculty of Ocean Engineering and Ship Technology, Gdańsk University of Technology, Gabriela Narutowicza 11/12, 80-233 Gdańsk, Poland
[2] Department of Physical Sciences, The Open University, Walton Hall, Milton Keynes MK7 6AA, UK

Received 15 June 2016 / Received in final form 18 August 2016
Published online 10 November 2016

Abstract. The field of Atomic and Molecular Physics (AMP) is a mature field exploring the spectroscopy, excitation, ionisation of atoms and molecules in all three phases. Understanding of the spectroscopy and collisional dynamics of AMP has been fundamental to the development and application of quantum mechanics and is applied across a broad range of disparate disciplines including atmospheric sciences, astrochemistry, combustion and environmental science, and in central to core technologies such as semiconductor fabrications, nanotechnology and plasma processing. In recent years the molecular physics also started significantly contributing to the area of the radiation damage at molecular level and thus cancer therapy improvement through both experimental and theoretical advances, developing new damage measurement and analysis techniques. It is therefore worth to summarise and highlight the most prominent findings from the AMP community that contribute towards better understanding of the fundamental processes in biologically-relevant systems as well as to comment on the experimental challenges that were met for more complex investigation targets.

1 Introduction

Development of next generation radiation therapy

In developed countries cancer is now the second most common form of death after cardiovascular disease. In Europe in 2012 approximately 3.45 million new cases were diagnosed and 1.75 million deaths were attributed to cancer [1]. Accordingly, European research into cancer treatment has been central to past, current and future national and transnational research strategies with the European Commission developing a European Partnership for Action Against Cancer with the aim of reducing the number of cancer cases by 15% by 2020 through the development of new methodologies for cancer treatment. Approximately half of patients receive radiotherapy as part of their cancer treatment, and indeed this type of therapy is second only to surgery in the treatment of cancer. However, radiotherapy is limited by the side effects it induces in the surrounding healthy tissues and/or the damage it can cause to vital organs (e.g. the kidney and brain). Several new approaches that enhance radiosensitivity within tumours have been proposed [2–8], which have the potential to provide a major impact on the delivery of radiotherapy to patients allowing lower doses to be applied with the same tumour mortality. Nowadays, two of the most promising approaches are hadron and nanoparticle-enhanced therapies, which allow the tumour to be directly targeted allowing both lower doses to be applied and reducing damage to neighbouriong healthy tissue and cells. Hadron therapy employing protons and carbon ions is now used in several medical centres worldwide. Nanoparticle therapy (NPT), while still in formative stage (early clinical trials), is showing promising results and it is expected that in future a combination of hadron and NPT will be the preferred (non-surgical) treatment plan.

Both Hadron therapy and NPT are driven by nanoscale phenomena [9] and therefore it is necessary to understand the fundamental processes, by which ionising radiation interacts with biological material and its constituent macromolecules [10]. Accordingly, in the last two decades a major topic of atomic and molecular physics has been to explore the dynamics of incident particle, like photons, ions or electrons, interactions with macromolecules [11] and their constituent components [12–18] in order to develop a molecular (nanoscale) model of radiation damage distinctive from the previous microscale energy deposition models that have been the basis of clinical radiotherapy protocols. Thus next generation

* Contribution to the Topical Issue "Low-Energy Interactions related to Atmospheric and Extreme Conditions", edited by S. Ptasinska, M. Smialek-Telega, A. Milosavljevic, B. Sivaraman.

[a] e-mail: smialek@pg.gda.pl

radiotherapy will be based on nanodosimetry rather than current microdosimetry, allowing lower doses being applied to patients.

Since realising the importance of DNA damage in cellular apoptosis, numerous studies have been performed in order to understand and predict the possible proceeding pathways and mechanisms. The very early investigations focused not only on experimental investigations of DNA damage levels [19–21], but also involved studies on the radical formation and attack on DNA molecule, using its building blocks as models [22–26]. This topic was already a subject of extensive reviews [27,28]. These experimental investigations were supported by theoretical modelling, aiding unravelling the possible mechanisms and complexity of registered damage [29–31].

When ionizing radiation is used to irradiate living cells, apart from the damage that results from the interaction of incident particles with biological matter, we also observe the effect that is due to formation of various kinds of secondary species upon irradiation of biomolecules and the medium surrounding them. These species include the products of radiolysis of water, like e^-(aq) (hydrated electrons), $H^\cdot$, $OH^\cdot$, H_2O_2 or H_3O^+ [32], but also a vast quantity of other reactive species, like ions and radicals, formed from the constituent biomolecules and DNA itself, among which the most abundant species that are produced in the cell are secondary electrons with energies between 1 and 20 eV [33]. These species can induce damage in the cell almost as efficiently as the incident particles of high energy. When the cellular environment is being investigated in the close proximity to DNA at the nanometric scale, it should be considered as an extremely concentrated solution, where all the suspended molecules play an important role in the secondary damage. Therefore, it is vital to investigate the interactions and damage mechanism between low energy electrons and DNA [34].

In the year 2000 the group of Leon Sanche published an astonishing result; they studied electron-induced damage in strands of DNA [35]. The DNA helix can be ruptured in two ways: one leading to a single strand break (SSBs), the other producing double strand breaks (DSBs). Boudaïffa et al. [35] showed that, contrary to expectation, low energy (<20 eV) electrons could produce both SSBs and DSBs (Fig. 1). The structures centred around 10 eV of incident electron energy, observed in the measured quantum yields of SSBs and DSBs as well as for the loss of supercoiled DNA form, were ascribed to result from dissociative electron attachment (DEA) to the constituents of DNA (i.e. thymine, water) that was later shown to be the dominant process for fragmentation of molecules of biological interest [13]. DEA mechanism follows a general scheme:

$$e^- + AB \leftrightarrow (AB)^{-\#} \rightarrow A^- + B, \qquad (1)$$

according to which, a molecule AB, after capturing a low energy electron (LEE), forms a transient negative ion (TNI) $(AB)^{-\#}$ that can further dissociate into an anion A^- and a neutral fragment B.

The investigators have subsequently showed that the observed resonant structures are dependent upon the target DNA base identity, DNA sequence, and incident electron energy [36]. They also showed that the efficiency of inducing strand breaks with low energy electrons is almost two times higher than with soft X-ray photons [37].

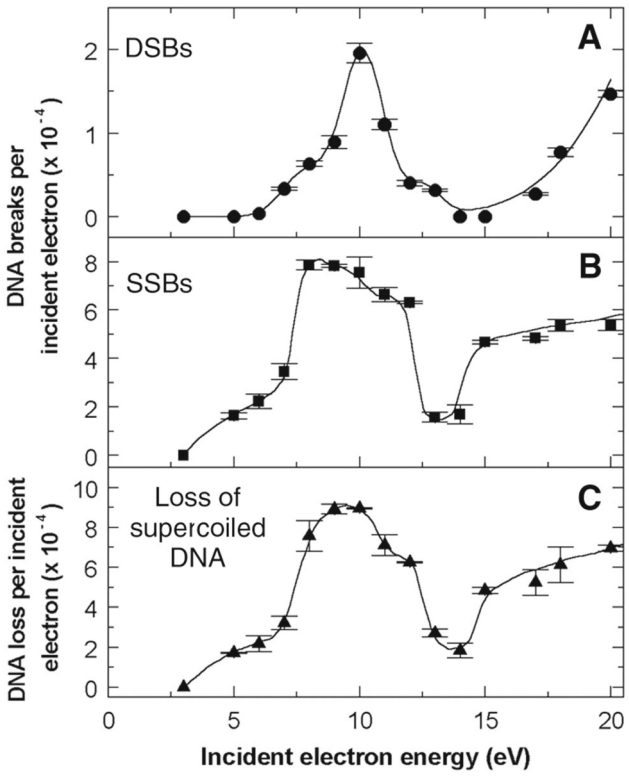

Fig. 1. Measured quantum yields, per incident electron, for the induction of DSBs (A), SSBs (B), and loss of the supercoiled DNA form (C), in DNA solids by low-energy electron irradiation as a function of incident electron energy; the curves are guides to the eye. From [35] Reprinted with permission from AAAS.

From there it was obvious that this mechanism plays a key role in the damage of DNA, thus extensive studies on DEA to DNA and its constituents [38,39], as well as other biomolecules [40–43] have been undertaken, both in the gas [44,45] and solid phase [46,47]. The topic of DEA to biomolecules has also been extensively reviewed by the experts in this topic [14,34,48,49].

The biodamage done by the secondary electrons together with free radicals and other reactive species, produced by ionizing high-energy primary radiation (X-ray, gamma ray, UV light, high energy electrons, or ions), is much more significant than that produced by primary radiation. Thus radiation chemistry and hence the models that underpin the radiotherapy protocols need to be based on atomic and molecular interactions, operating on the nanoscale rather than the traditional macroscale picture. This led to an explosion of experimental studies that explored electron, ion and photon interactions with biomolecules such as the nucleobases, from which DNA is built [50] and provided theory with enormous challenges

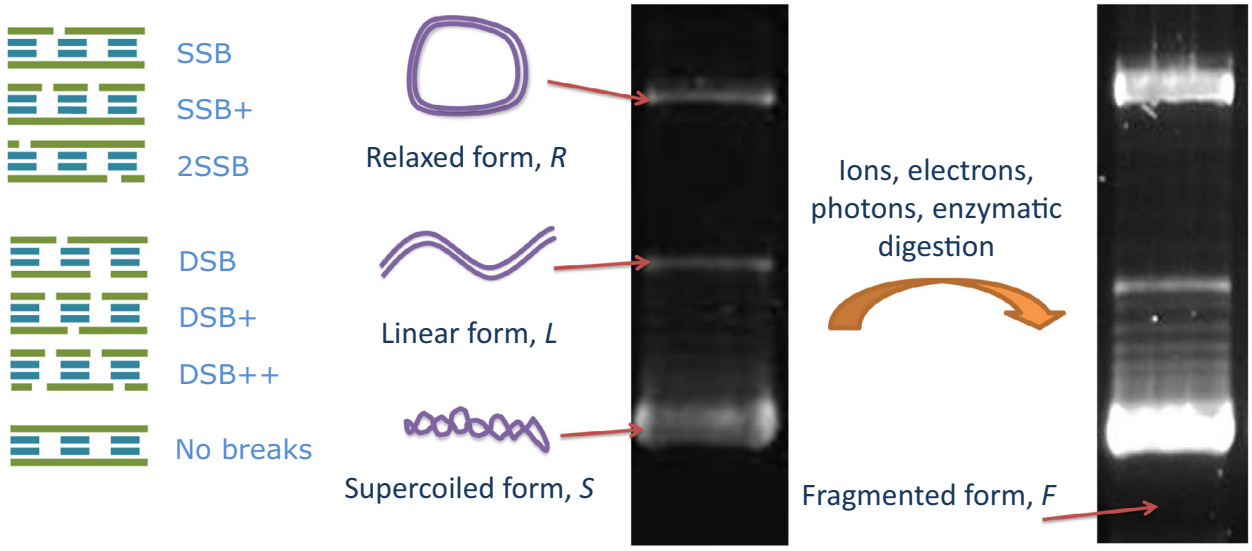

Fig. 2. Three main forms of plasmid DNA topology: relaxed, linear and supercoiled, representing different types of lesions, developed on agarose gel in a form of characteristic bands. After staining the gel with a fluorescent dye coupled to DNA, the emission intensity of the respective bands is measured, thereby determining the amount of the resulting single and double breaks.

to model interactions with such complex molecular targets [51,52].

Central to the quantification of the relationship between the amount of energy deposited within a given region of the DNA helix and the type and severity of the damage that is produced, are fundamental studies of the molecular physics of biological systems. Such studies are extremely challenging since they require a combination of techniques and experience between the AMP and biosciences communities, two communities that, until recently, have not collaborated and whose experimental methodologies are very different.

2 Development of sample preparation and damage analysis methods for DNA irradiation experiments

For fundamental radiation damage research it has been central to develop the experimental protocols that quantify molecular scale damage in macromolecular systems (primarily DNA). Performing molecular physics experiments with biomolecular targets is a significant challenge since the results may rely on transfer of biomolecular protocols and analysis techniques to AMP experimental systems and procedures. In many cases the results obtained from such experimental studies may vary, depending on the experimental conditions we use and the initial preparation procedures of the biomolecular/biological target which, unlike traditional atomic and molecular targets (high purity gases) have an inherent variability. How does such a variability influence our findings? Are we using the correct analytical methods? How do we quantify the systems that are actually being investigated? Do we understand the models that are being used to fit the experimental data? Are we sure that the values of cross sections and constants we assume, are well-established?

These questions are central to the development of the next generation of radiotherapy experiments. Trying to at least partially answer the above questions, some new methodologies for the next generation of experiments exploring DNA damage had to be developed. For such studies, plasmid DNA is frequently used as it is easy to handle and, due to its three conformers (supercoiled, relaxed and linear), provides information on supercoiled molecule relaxation and double strand break formation, that can be easily seen by agarose gel electrophoresis (AGE), as demonstrated in Figure 2.

AGE detects changes in plasmid DNA conformations, with SSBs leading to circular plasmids with a relaxed conformation while DSBs result in linear plasmid DNA. Such a methodology is suitable for determining the amount of DSBs but when used to quantify SSBs it invokes an implicit assumption, namely that there is just one SSB per molecule and that SSBs are present only in molecules that form a relaxed band on the gel. Such an assumption does not have to be true because the molecules forming the relaxed and linear bands can both contain multiple SSBs. This situation is illustrated schematically in Figure 2, which also shows where the bands will appear on the gel. Any underestimation of the number of SSBs in the irradiated samples may result in errors in the interpretation of the damage formation process and can lead to an incorrect characterization of processes leading to DSB formation, which is a crucial event for determining cell apoptosis. Moreover, it will be shown in Section 2.1, how crucial the proper assignment of DNA lesions is for modelling of radiation damage.

2.1 Obtaining the basic parameters of DNA damage through fitting experimental data with theoretical models

When handling the experimental results it is critical to extract as much information as possible. In order to achieve that, an employment of some accurate and adequate models is required [53].

Probabilistic models that are still widely used, were derived in order to analyse the experimental outcomes of DNA irradiation studies and were somehow first developed to suit the experimental procedure that was chosen by investigators. The earliest DNA damage studies [19–21] employed sucrose gradient centrifugation to analyse the strand breaks and focused on transitions from relaxed, R, to linear, L, DNA form. These experimental studies have been supported by theoretical DNA damage models in order to distinguish between radiation damage created by direct irradiation, e.g. with incident high energy photons, and damage induced by indirect processes, e.g. engendered by hydroxyl radical formation and attack. The main aim of irradiation in radiotherapy is to obtain the highest levels of double-strand breaks, lethal to living cells, and to accumulate the single strand breaks that this way can lead to DSBs formation, when the single-strand lesions appear in both DNA helix strands within a small distance, usually denoted as a or h. This distance is measured in base pairs for double stranded DNA molecule. Together with changes in DNA conformation, this distance has become one of the most important parameters to be determined in the samples exposed to damaging agents of various kinds. Simultaneously, investigations on the probability of breaking a DNA strand by incident particles have been conducted. The very first studies did not take into account parameters like random lesion distribution within both strands or the strength of phosphodiester bonds in the DNA backbone [19], and the experimental data fitted with the theoretical model that was developed gave a value of $a = 2$. Also, since only transformation from R to L form of DNA was investigated, many factors could have been simply overlooked. Later research revealed how single-strand lesions are deployed between strands of DNA molecule and their influence on DSBs formation [20]. It was also found that the initial conformation (R or L) of the plasmid molecule had a great impact on the yields of damage obtained from irradiation [21] with the R form being far more susceptible to radiation damage.

In all cases the experimental results obtained for various types of damaging agents showed some discrepancies in the determination of the a value. Also, since a very simple system was analysed, the simplified approach, based on Poisson distribution, was employed in order to model the damage observed. When a new experimental method, agarose gel electrophoresis was developed for analysis of DNA damage induced by radiation [54], the possibility of investigating the decrease in supercoiled, S, DNA levels and to follow dose-dependent quantitative changes in all three DNA forms arose. The relationship between various topological forms of DNA as well as levels of damage that could be detected with this new method were derived. Once the new technique, AGE, was used, it was found that the breakdown mechanisms are far more complicated than previously assumed and thus more complex models must be sought.

The first damage model that fully described the changes between all three plasmid DNA forms after irradiation was presented by van Touw et al. in 1985 [54]. This model considered the binomial distribution of SSBs along one DNA strand and originated from a simplified case developed earlier by Freifelder and Trumbo [20]. In both cases the authors tried to relate DSB formation to the initial levels of SSBs. In the latter case, this relationship was made without distinguishing DSB formation as being the result of a single- or multiple-hit event, whereas in the former case, both pathways and their probabilities were established. Therefore, the number of SSBs, P_S, and DSBs, P_D, per DNA molecule, resulting from a single event should exhibit a linear response with respect to the radiation dose, D

$$P_S = P_S^0 + \frac{D}{D_{37S}}, \tag{2}$$

$$P_D = P_D^0 + \varepsilon \cdot \frac{D}{D_{37S}}, \tag{3}$$

where P_D^0 and P_S^0 are the average number of DSBs and SSBs per DNA molecule at zero dose respectively, D_{37S} is the dose at which there is, on average, one SSB per DNA molecule (37% survival rate) and ε is the efficiency, with which a single hit DSB is formed as compared to a SSB.

As the damage as such does not have to have a uniform distribution between two strands creating a double-stranded DNA molecule, a binomial distribution of damage needs to be considered. Therefore, to model DNA damage and the transition of the supercoiled DNA form into relaxed and linear ones, the damage model presented by van Touw et al. [54] uses a binomial distribution to evaluate the average number of multiple-hit DSBs, P_{DS}, being derived as a function of SSBs formation

$$P_{DS} = \left(\frac{P_S}{2}\right)^2 \cdot \frac{2a}{L}, \tag{4}$$

where a is a distance within which two SSBs situated on the opposite strands will create a DSB and L is a contour length of the DNA molecule.

Using a binomial distribution to describe the probability of causing either a SSB or a DSB by a single projectile and, as a consequence of a moderate magnitude of successful events, approximating the probability with a Poisson distribution it is possible to obtain a set of simplified expressions describing changes in the average numbers of supercoiled, N_S, relaxed, N_R, and linear, N_L, DNA molecules upon irradiation

$$N_S = \exp(-P_D) \cdot \exp(-P_S), \tag{5}$$

$$N_R \simeq \exp(-P_D) \cdot [\exp(-P_{DS}) - \exp(-P_S)], \tag{6}$$

$$N_L \simeq (P_D + P_{DS}) \cdot \exp(-P_D) \cdot \exp(-P_{DS}). \tag{7}$$

Such a simplification can be used in case of low P_S values and it was shown that for investigations of hydroxyl

radical attack [55] that this condition was fulfilled, thus the model may be implemented for DNA damage modelling. In addition, when this simplified case is being analysed, and the distribution of SSBs between two DNA strands is not being distinguished but treated as equally distributed between the two stands, the accumulation of DSBs as a result of SSBs accumulation, P_{DS}, can be written as [20]

$$P_{DS} \simeq \frac{2a+1}{4L} \cdot P_S^2 \tag{8}$$

and the increase in the total number of DSBs as a result of increasing dose of radiation can be approximated by a simple linear-quadratic expression [56]

$$N_L = \alpha \cdot D + \beta \cdot D^2. \tag{9}$$

Later, it was shown by Siddiqi and Bothe [56], who used a low angle laser light scattering on denatured DNA fragments to assess γ-radiation damage to DNA, that the original approximation is sufficiently accurate to model the damage levels within their experimental uncertainty.

Another interesting point was raised by Boudaïffa et al. [57], who also noted that in certain experiments, a penetration depth of the incident radiation needs to be accounted for and thus introduced a correction factor to be used when plotting N_S, N_R and N_L

$$N_{X_{corr}} = [h \cdot N_X + (H-h) \cdot N_{X0}]/H, \tag{10}$$

where $N_{X_{corr}}$ is the corrected value of the initial, N_{X0}, and recovered after irradiation X-form of DNA ($X = S$, R or L) for the effective range for strand breaks formation, h, with respect to the thickness of the sample, H.

When, on the other hand, P_S values are high, more complex methods need to be employed, such that not only the three basic topological forms of plasmid DNA are considered, but also fragmented form that arises from accumulation of DSBs in DNA molecules, need to be accounted for. This form that arises from further fragmentation of linear molecules, was also investigated and the loss of linear molecules due to multiple DSBs (MDSBs) formation was described simply by measuring the quantity of the material missing from the sample upon treatment with respect to untreated control [58]. This fragmentation was also considered with respect to the DSB in DNA being a result of a multiple SSBs accumulation or by simultaneous cleavage of both strands by a damaging agent. Such approach has to be undertaken when fragmented form is detected after irradiation experiment or chemical treatment of DNA sample [57].

Nowadays sophisticated computational methods are in use. Due to their complexity it is now possible to deal not only with simple break formation, but also to account for the influence of irradiation of the DNA environment, i.e. in a living cell, and to simultaneously account for secondary species attack [59–62]. Moreover, an accurate examination of the mode of action of various incident particles can be performed at the same time [14,63]. Another interesting and promising way of analysing the damage formed upon irradiation is the multiscale approach [64]. This is a physical phenomenon-based analysis of the situation that leads to radiation damage and was designed to consider all relevant effects on a variety of size and time scales and to develop an approach to the quantitative assessment of biological damage, including also chemical effects in the irradiated system.

2.2 VUV induced damage in DNA

As mentioned before, almost all of the molecular physics experimental studies of photon-, electron- and ion-induced damage to DNA have employed AGE to assess the amount of SSBs and DSBs in the irradiated samples (e.g. [57,65,66]). From Section 2.1 it is already clear that P_S and N_R have to be separated in order to accurately calculate the damage parameters. For example, if the number of SSBs is underestimated, correlation between their appearance and DSB formation cannot be established. Thus DSBs will be interpreted as a result of a single event rather than a series of two independent subsequent interactions between incident particles and DNA molecules.

The significance of VUV-radiation-induced DNA damage has been known for a long time, and extensive studies have been undertaken to understand the mechanisms by which the damage to DNA from VUV radiation takes place and to predict the possible damage pathways (for examples, see Refs. [65–67]). Folkard et al. [68] reported results for VUV irradiation of an aqueous solution of plasmid DNA and showed that there is a strong influence of the medium on the damage induced. Their results showed a large increase in the damage yield compared to dry plasmid DNA. By introducing a scavenger into the solution, Folkard et al. demonstrated that this difference may be ascribed to hydroxyl radical-induced damage; the amount of damage was reduced by more than half when the scavenger was present. In this case, the damage to DNA samples was expressed in terms of loss of supercoiled DNA and DSB formation, but no quantification of SSB formation after irradiation was performed despite SSBs usually being the most prevalent damage, as seen by the amount of relaxed DNA by AGE.

Therefore, to accurately determine the level of SSBs in samples that have been exposed to VUV radiation, an alternative analysis method based on the TUNEL (Terminal deoxynucleotide transferase dUTP Nick End Labelling) assay, which is used for SSB labelling with a fluorescent probe in cellular DNA to detect apoptotic cells [69] was developed [55]. In this work, the assay has been translated into an ELISA (Enzyme-Linked ImmunoSorbent Assay) – based conditions, in which purified DNA immobilised on plates can be used instead of cells. A schematic arrangement of this assay is presented in Figure 3.

The 3′-hydroxyl ends of the DNA sugar-phosphate backbone, which are a likely outcome of SSB formation [70], are labelled with brominated deoxyuridine triphosphate (BrdUTP) nucleotides in a reaction catalysed by the terminal deoxynucleotidyl transferase (TdT) enzyme. This is followed by an incubation with an commercially available anti-BrdU mouse monoclonal antibody linked to horseradish peroxidase (HRP) that then

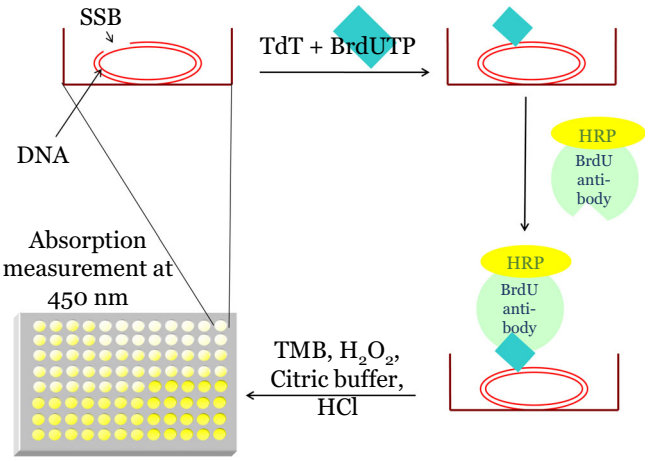

Fig. 3. General scheme for the ELISA assay.

catalyses the oxidation of species such as 3′,3′,5′,5′-tetramethylbenzidine (TMB) to give a coloured product, which then can be detected spectrophotometrically.

In the first application of the TUNEL/ELISA methodology to molecular physics studies, VUV light-induced damage of DNA (using 170 nm light derived from a synchrotron source) was investigated [55]. By comparing the results obtained from TUNEL/ELISA with results obtained using AGE, it was then possible to explore and confirm the assumption that more SSBs are being produced in the DNA after irradiation than can be assessed with AGE.

Analysing the VUV irradiated DNA the number of SSB per DNA molecule in the irradiated sample, P_S, can be plotted as a function of radiation dose, D, as shown in Figure 4a. It can be seen that the increase in those lesions with respect to the dose is linear. When the experimental data are fitted with equation (2), the dose D_{37S}, at which, on average, each DNA molecule possesses one SSB, is calculated to be 9.21 ± 0.15 Gy (see Fig. 4a). On the other hand, when the total number of SSBs obtained from the ELISA is plotted as a function of the total number of relaxed molecules that were detected from the gel (Fig. 4a, top scale), the increase in the lesions of interest is exponential with the increasing amount of relaxed molecules in the irradiated samples. Such behaviour demonstrates that for the relaxed molecules the probability of damage and appearance of SSBs is greater than for the supercoiled molecules.

Often, a method based on using a slope of the linear regime of relaxed DNA form appearance is used to calculate e.g. effective yields of SSBs formed upon irradiation [71]. When plotting number of SSBs per DNA molecule against the radiation dose obtained from both methods that were our subjects of investigations, it is clearly seen, that the underestimation of the damage levels is already significant at very low doses of radiation (Fig. 4b). For the data presented here the discrepancy would be of a factor of two at the dose of 5 Gy. Thus if AGE is used alone it will lead to an underestimate in the number of SSBs and hence misrepresent the amount of induced damage which in turn has consequences for cellular repair activity.

Furthermore, when number of supercoiled molecules is plotted against the number of SSBs per one DNA molecule, using equation (5) corrected with expression (10) it was possible to obtain a value for the efficiency, with which a single hit DSB is formed as compared to a SSB, ε (Fig. 5a). In this case, the value yielded zero, which means that the formation of DSBs is a result of two consequent events rather than of the single hit. Taking into account that here we consider a hydroxyl radical attack on DNA, this conclusion is very likely to be true.

Next, when plotting the DSBs obtained from AGE as a function of corresponding levels of SSBs found with the ELISA, it is possible to conclude that in case of hydroxyl radical attack, DSBs formed after a single projectile attack do not play a significant role. We fitted the linear-quadratic model (9) corrected for the penetration depth with (10) to the experimental data to retrieve the values for α and β parameters (see Fig. 5b). As seen from there, only a part of equation that corresponds to DSBs being formed as a result of two independent events, i.e. with a non-zero β parameter, is valid. Also, the value for the smallest distance within which two SSBs from opposite strands will create a DSB was derived using equations (7) and (8), yielding either 42 ± 15 bp or 43 ± 16 bp depending on the damage model used. Although the literature quotes the value of 10 bp for a formation of DSB as a consequence of two independent SSBs, i.e. the approximate length of one helical turn, it has to be kept in mind that this is only valid, when no other types of lesions are present in DNA strands. In case of hydroxyl radical attack it is known that locally multiply damaged sites are formed with base damage occurring 2.7 times more often than SSB [72]. Thus, in case, when between two SSBs there are other types of lesions that weaken the hydrogen bonding between the two DNA stands, it is possible that this distance will be larger. The value quoted here is also in agreement with that of approximately 43 bp reported by Siddiqi and Bothe [56], who likewise investigated hydroxyl radical damage to DNA, formed after photon irradiation.

The most recent advances in atomic force microscopy allow now direct observation and single DNA molecule manipulation with employment of so-called DNA origami templates [11]. Therefore it became possible not only to detect but also to accurately quantify the yields of oligonucleotide strand breaks formed directly upon irradiation with electrons [73] or photons [74].

2.3 Preparation of DNA films for vacuum studies of DNA damage

Since the pioneering work in the year 2000 from the group of Boudaïffa [35] there have been several attempts to repeat and extend these studies but with varying degrees of success and results have shown significant differences [75–77]. These differences are mainly due to the difficulty that AMP groups have in preparing DNA films for irradiation.

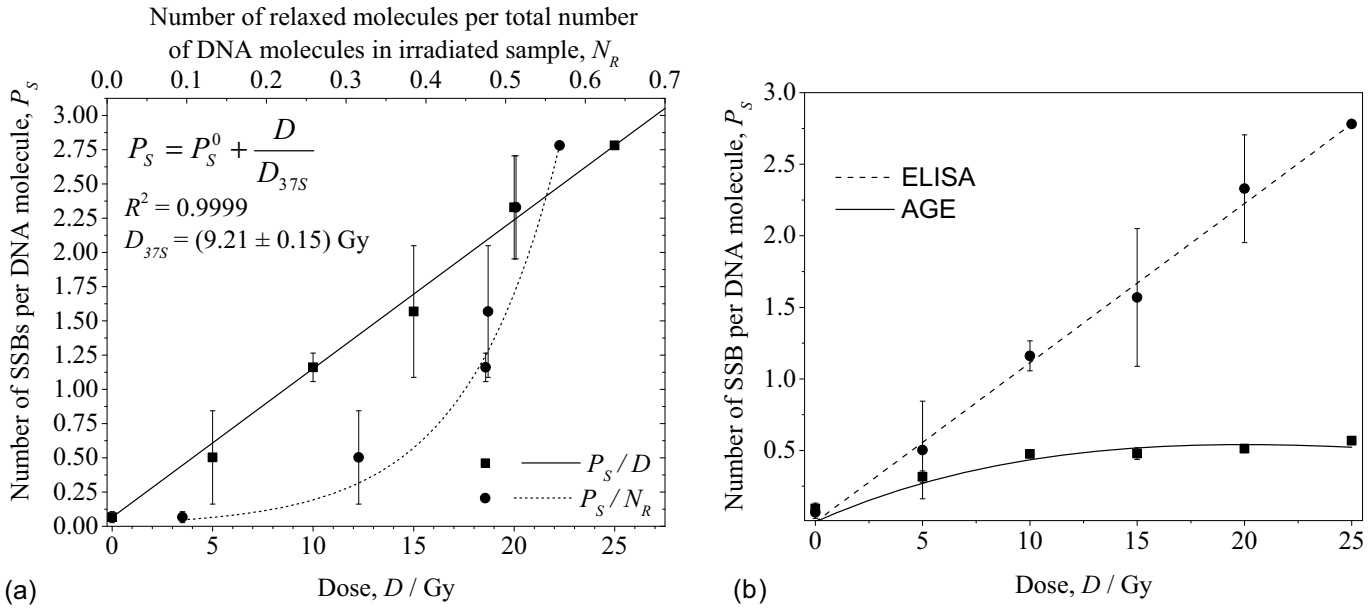

Fig. 4. a) The number of SSBs induced in the VUV-irradiated sample, assessed with ELISA, increases linearly with radiation dose delivered to the sample, whereas the number of SSBs per single DNA molecule increased exponentially (dashed line) with the number of relaxed molecules present in the sample after irradiation; b) number of SSBs as assessed from AGE (solid line) and ELISA assay (dashed line). Error bars are ±1 SD.

To study electron, ion or photon interactions with biological material under vacuum conditions, such as DNA, suitable preparation of the sample is required in order that films are reproducibly formed and are stable under the experimental conditions required, usually a high or ultra-high vacuum. For the experimental results to be quantitative it is of great importance for the biological material to remain as intact as possible during the preparation process. One of the most important issues to be dealt with is the removal of constituent water from DNA molecules during sample evacuation. It has been shown that the subtraction of such water initially leads to damage of the molecules in the form of single (SSB) and double strand breaks (DSB), and eventually complete decomposition of the DNA molecule to its basic building blocks, the nucleotides and nucleosides [78].

To avoid DNA decomposition, the solution containing the molecules that are to be investigated must contain other species that can stabilize the structure during the drying process and prevent the removal of constituent water molecules.

The most commonly used compounds for DNA stabilisation are trizma base (tris) [79] and ethylenediaminetetraacetic acid (EDTA) [80]. Both molecules are much more complex than simple hydroxides, possessing three (trizma base) and four (EDTA) hydroxyl groups, which may, depending on the experimental conditions, interfere with projectile-DNA molecule interactions while acting as a protectant. This effect was also confirmed recently by Kumar et al. [81]. Therefore, simpler stabilizers must be sought. The temperature and the environment at which films are made are also important factors in the preparation process. Freeze-drying is commonly used in the preparation of samples intended for use in high vacuum conditions. This technique causes lyophilization of liquid samples and is used in most cases to prevent DNA aggregation during solvent removal [82]. Nonetheless, this procedure may influence the formation of the film causing development of DNA network [79]. Until recently, there had been no systematic study of the role of such adducts in the morphology of the prepared DNA films. Similarly, although commonly used, no studies have been performed to assess how the freeze-drying technique influences the DNA film formation in the presence of external factors, like stabilizers or the temperature of the substrate.

In order to obtain the information on how to control the film preparation process, the influence of substrate temperature during the freeze-drying process on film formation, survivability rates of the plasmid DNA under vacuum conditions and the influence of potential stabilisers on the film formation were explored. Previous studies have reported films that have been formed with the substrate kept at temperatures varying from room temperature [80] to liquid nitrogen temperatures [35] while depositing the liquid sample. The influence of stabilisers such as sodium, potassium, magnesium and calcium hydroxides required to maintain the supercoiled form of DNA in the formation of films [84] was explored along with investigation of how DNA films are affected by these stabilisers when varying the substrate temperature [83].

Since tantalum has already been shown to be a good choice of a substrate for the vacuum irradiation studies of interactions between DNA and LEE [85], in the investigations of DNA film properties [83,84] Ta foil was also selected as a substrate. The high atomic number of Ta reduces secondary electron emission upon low energy

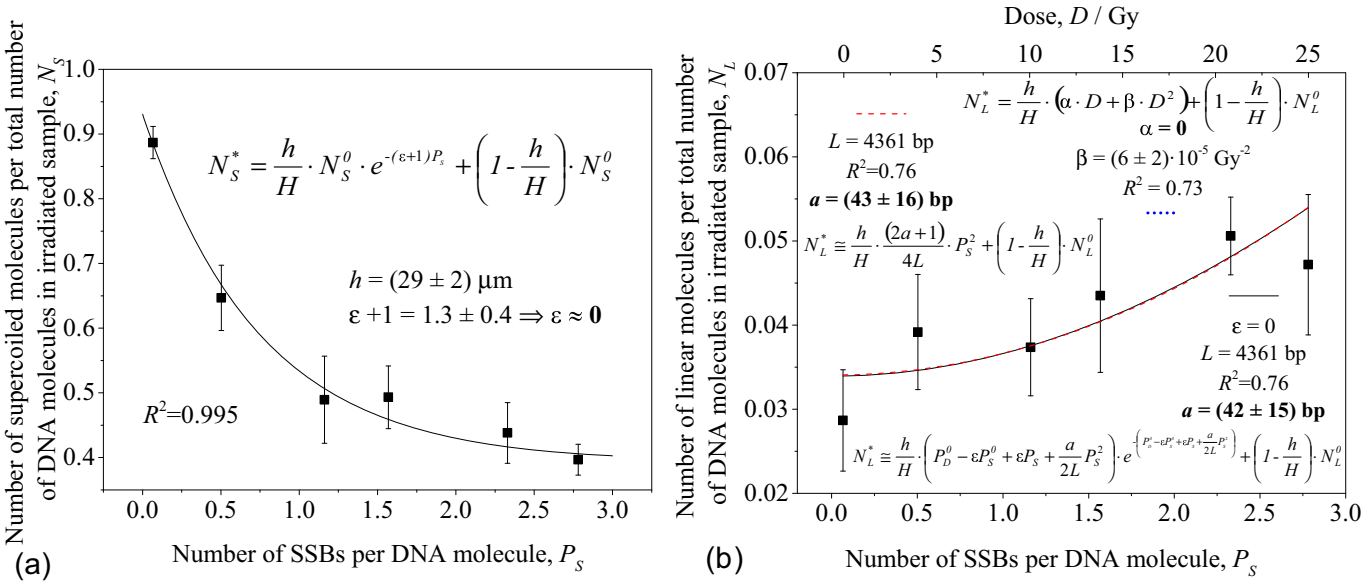

Fig. 5. (a) Number of supercoiled molecules present in the sample with respect to the number of SSBs formed upon irradiation was fitted with (5), giving the value of $\varepsilon = 0$ [55]; (b) the number of DSBs per single DNA molecule, assessed by AGE, plotted as a function of number of SSBs per DNA molecule and radiation dose, fitted with: (7) – black, solid line, (8) – red, dashed line and (9) – blue, dotted line; the linear coefficient α was determined to be zero and distance $a = 42 \pm 15$ bp. In all cases, a correction for the penetration depth h with respect to the total thickness of the sample H was applied.

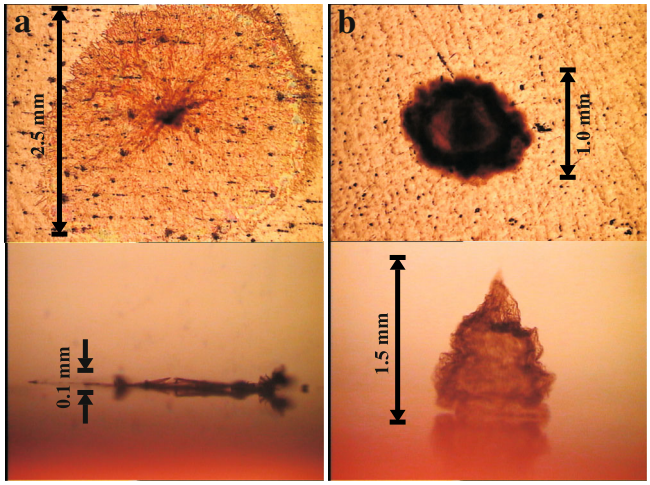

Fig. 6. Images from light microscope of top view (top line) and side view (bottom line) of DNA films prepared from 2 μL UHP H_2O containing 100 ng plasmid DNA, placed on the substrate at a) –10 °C and b) –20 °C (modified from [83]).

electron irradiation, and the tantalum oxide layer that is formed on the metal surface creates a stable, chemically inert surface, minimising DNA-substrate interaction. Ta foil was polished on fine sand paper wheels, cleaned in an ultrasonic bath in pure ethanol and blow-dried with dry N_2 to ensure even and uncontaminated contact surface. No damage was observed due to the contact of plasmid DNA with the surface of the substrate.

Figure 6 shows light microscope images obtained for DNA films from solutions containing 100 ng DNA in 2 μL of ultra-high purity (UHP) H_2O, deposited at (a) –10 °C and (b) –20 °C on the tantalum substrate. The top images are top views of the prepared films, and the lower images show the side view of both films. It can be seen that the film prepared at –10 °C forms a large, flat circle of approximately 2.5 mm in diameter and with a height of about 0.1 mm. The film prepared at –20 °C formed a compact structure of 1 mm in diameter and a height of approximately 1.5 mm. From these observations it can be concluded that the shape of the DNA film formed using the freeze-drying technique is strongly dependent on the temperature at which the liquid sample is placed on the substrate.

For samples deposited at substrate temperatures higher than –20 °C, the droplet can spill over the surface of the substrate before cooling to the freezing point. At lower temperatures, the small volumes of liquid sample used in the experiment freeze immediately upon touching the cooled surface. After the water has been removed in the evacuation process, the dried DNA film retains the shape of the initial frozen sample droplet.

Further investigations of such films using a scanning electron microscope (SEM, Fig. 7) were performed and irregular, cracked surfaces in the samples deposited at the temperatures above freezing point and very compact and squashed shapes with a characteristic, dense "rim" for samples prepared at –20 °C were observed. In neither case was the film uniform enough to assume an even molecular distribution. Also the surface area of the film was far from originally assumed.

At the same time it was also observed that the samples of plasmid DNA suspended in UHP H_2O do not survive at the low pressures necessary for low energy electron irradiation. Whether the vacuum levels were high or low,

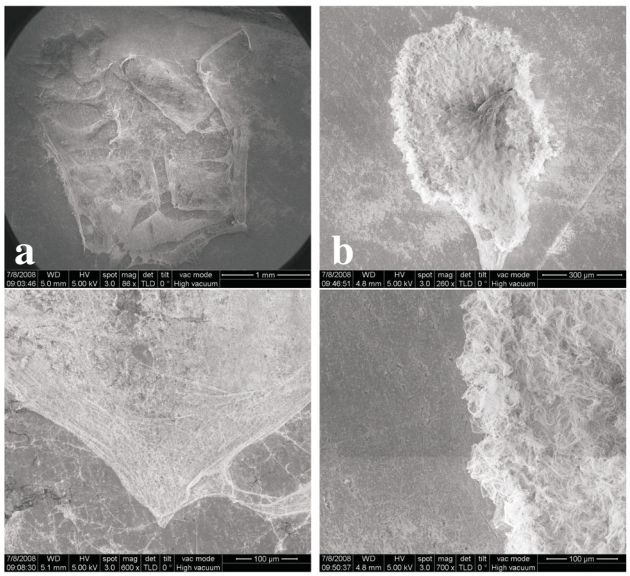

Fig. 7. Images of DNA films prepared from 2 μL UHP H_2O containing 100 ng plasmid DNA, placed on the substrate at a) +4 °C and b) –20 °C, together with close-ups of the central area and edges of the samples.

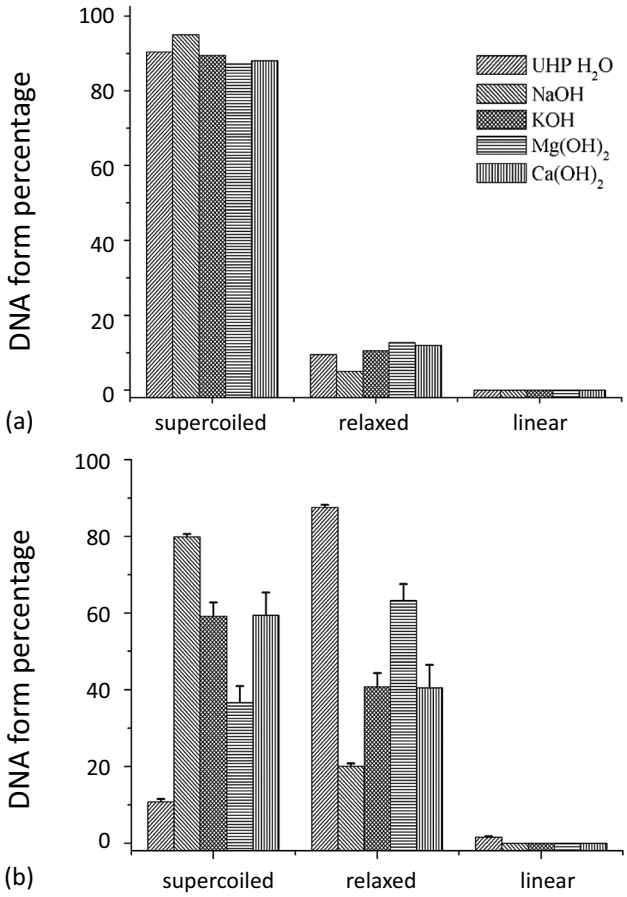

Fig. 8. a) Assessment of base influence on plasmid DNA stock solutions; the smallest loss of supercoiled DNA form is seen with NaOH solution, which even resulted in the DNA molecules being more stable than DNA suspended in only UHP H_2O; b) loss of the supercoiled form of plasmid DNA and formation of SSBs and DSBs arising from different basic solutions after evacuation of the samples at 10^{-5} mbar for 16.5 h at +4 °C substrate temperature (modified from [84]).

most of the supercoiled form of the starting material was immediately lost after applying vacuum.

Following these experiments we sought to develop an experimental methodology that would produce well-characterised DNA films. In many previous studies the samples were stabilised with the use of tris and/or EDTA that are rather complex molecules. The most reasonable approach was to introduce compounds of the simplest possible composition in order not to introduce more variables into the system. Accordingly, mono- and dicationic bases containing sodium, potassium, calcium and magnesium were tested. From the AGE test, shown in Figure 8, sodium hydroxide proved to be the best choice, since not only it has no effect on the samples before exposed to the experimental conditions (a), but also the levels of DNA damage obtained upon evacuation of the system were the lowest (b). This was also supported by the outcomes of our SEM investigations, which revealed that the most uniform films were produced from plasmid DNA suspended in NaOH solution. The shape and surface area of the deposited film was found to change with the temperature of the substrate during the deposition (Fig. 9a), as well as with the quantity of NaOH added to the sample (see Figs. 9b and 9c).

The effect of the commonly used Trizma base on the formation of DNA films was also explored (Fig. 10). DNA films prepared at +4 °C (a) and –5 °C (b) were compared by measuring the total area and the distribution of material within the central area and edge of the sample. The greatest differences can be seen at the edges. The sample prepared at +4 °C has a much higher concentration close to a well-defined edge than the sample prepared at –5 °C. The material distribution within the central part of the sample is uniform for the +4 °C film, but the film prepared at a lower temperature formed small aggregates of various sizes, with the largest of these close to the centre of the sample.

Having identified the above problems with the standard evaporation procedures, these results have led to the development of the new preparation techniques for irradiation studies of DNA films by several groups. For example in 2011, a group of Professor Fromm published a new protocol for an uniform plasmid films preparation, employing 1,3-diaminopropane (DAP), Boulanouar et al. [86]. The films, containing DAP bridges (Fig. 11), were found to be much more uniform than the ones obtained through standard evaporation procedures, described above.

The authors also admitted struggling with sustaining the plasmid DNA in the supercoiled form under vacuum conditions. To overcome this issue, a standard

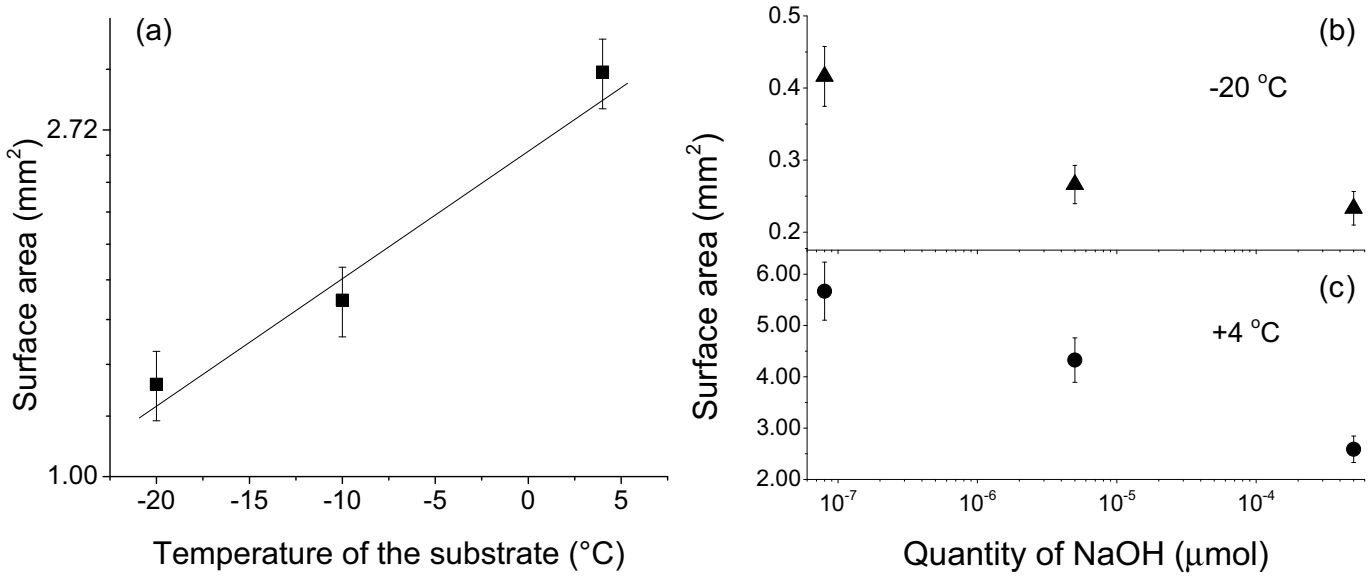

Fig. 9. a) An increase in sample area with increasing temperature of substrate during film preparation, calculated from samples containing 1 μL UHP H_2O with 100 ng plasmid DNA + 1 μL NaOH pH 8.0 placed on the tantalum support at +5 °C, –10 °C and –20 °C; the error bars shown on the graph represent uncertainty of the evaluation of the surface area of the sample; the solid line represents a guide to the eye; b) a decrease in sample area with increasing base content in samples containing 100 ng DNA in: 6 μL UHP H_2O, 1 μL UHP H_2O + 5 μL NaOH pH 8.0 and 1 μL UHP H_2O + 5 μL NaOH pH 10.0, prepared at a substrate temperature of –20 °C (triangle symbol) and (c) +4 °C (round symbol); the error bars shown on the graph represent uncertainty of the evaluation of the surface area of the sample (modified from [83]).

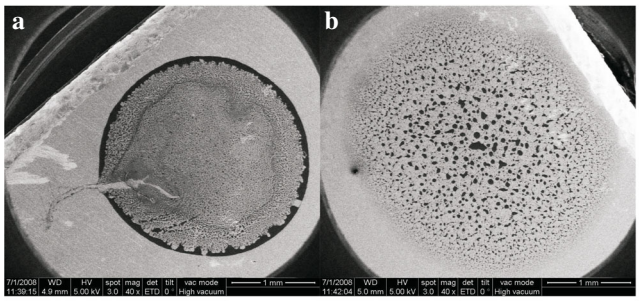

Fig. 10. 100 ng of plasmid DNA in 2 μL of 5 mM Tris-Cl buffer placed on the substrate at a) +4 °C and b) –5 °C.

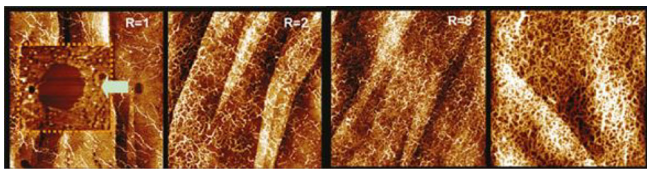

Fig. 11. AFM (5×5 μm) tapping mode images of layers composed of [plasmid DNA·Dap^{2+}] complexes at various ratios R of Dap^{2+} to phosphate groups on DNA backbone and supercoiled DNA = 20 ng/μL (adapted with permission from [86]. Copyright 2016 American Chemical Society).

tris-EDTA buffer as a stabiliser of DNA was used (Fig. 12). From there, a successful irradiation of DNA films both under vacuum and atmospheric conditions was conducted [87,88].

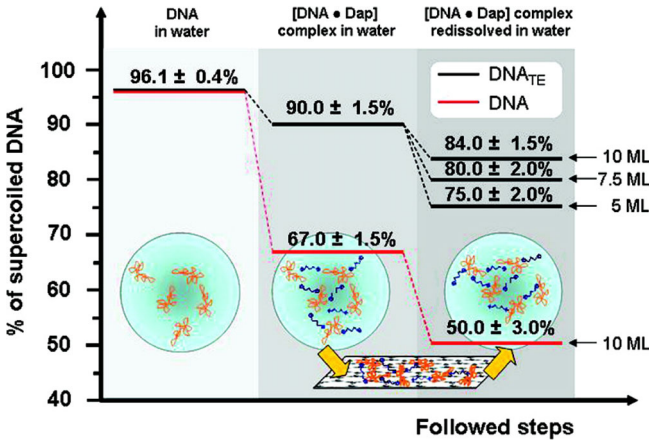

Fig. 12. Summary of the various average percentages of supercoiled DNA after the different steps necessary to release DNA-Dap complexes in water. The thicknesses of the layers are expressed in terms of monolayers (ML); one ML typically corresponds to 2.2 ± 0.5 nm. Thin layers are more fragile than thicker ones (Reprinted with permission from [86]. Copyright 2016 American Chemical Society).

2.4 Measuring the density of DNA films

The investigations of the morphology of DNA films published in [84] and [83] triggered another question: if the DNA film is not as compact as we believed, how does the density of the film change as a function of morphology?

In order to characterize the interactions between DNA molecules in a film and incident particles it is necessary

Table 1. Comparison of values for CT DNA density that can be found in the literature; (bdg is buoyant density gradient) (adapted from [102]).

Source	Method	Density (g/cm^3)
Śmiałek et al. [102]	Interferometry	1.41 ± 0.03
Astbury [99]	Gravitometry	1.63
Franklin and Gosling [100]	Gravitometry	1.625 ± 0.002
Inagaki et al. [89]	Interferometry	1.35
Weidlich et al. [101]	Crystallography	1.64
Votavova and Sponar [103]	CsCl-netropsin bdg	1.7
Thiery et al. [104]	CsCl bdg	1.7033 ± 0.0002
Macaya et al. [105]	Cs_2SO_4 BAMD bdg	1.7085
Filipski et al. [106]	Cs_2SO_4 bdg	1.697

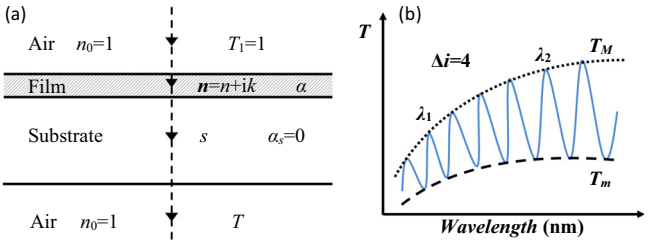

Fig. 13. For a light absorbing thin film supported on a thick, finite, transparent substrate a) the interference effects will give rise to the transmitted signal producing interference fringes, confined by two envelopes T_M and T_m b). λ_1, λ_2, and Δi according to the text [102].

to measure both the optical and dielectric properties of DNA [89] and, in particular, determine its density. The accuracy of the measurement of DNA density is important when other parameters such as refractive index, extinction coefficient, oscillator strength [89,90], energy loss function [91–94], electron mean free path [95], effectiveness of DNA strand breakage [96], electron [97] and proton [93] stopping power, or various cross sections for DNA-electron and photon interactions [4,82,97,98] are to be determined. Measurements of the density of dry DNA films have previously been performed using a variety of methods, with the results strongly related to the method used (see Tab. 1) [89,99–101].

The most commonly used value of the density of calf thymus (CT) DNA and other genomes (including human) as well as plasmid DNA is 1.7 g/cm^3 [103,105–108]. This value was measured using the buoyant density gradient, which is commonly used to determine the unknown density of a component against the known density of a solvent. This technique resolves a sample into components of differing buoyant densities upon centrifugation. The term buoyant density refers to the fluid density, in which the sample particles manifest no tendency either to float or to sediment. The drawback of this technique is that it strongly depends on the solvent [109] and the temperature at which the procedure is carried out [110]. Moreover, the density of DNA established using this method refers to molecules in an aqueous environment, which is obviously not the case for the films prepared either under vacuum or air dried. To date there are no consistent measurements of the density of dried DNA films, but the density is expected to be between that in solution and the density of powders of nucleosides or nucleotides (e.g., adenosine 0.998 g/cm^3).

In order to determine a new value for the density of dry DNA films as prepared for irradiation studies, a method based on the measurement of interference fringes of transmission spectra from thin DNA layers was used [102]. A weakly absorbing uniform thin film of thickness d was formed on a transparent substrate (in our experiments – magnesium fluoride window) with a thickness several orders of magnitude larger than the film (Fig. 13a). The film was prepared through a gentle evacuation of aqueous solution of CT DNA with a water pump. The different refractive indices of the elements in this system-air, film, and substrate-give rise to multiple reflections from the interfaces. Interference effects due to the film, as the reflected waves constructively and destructively interfere, give rise to fringes in the resulting transmission spectrum (Fig. 13b). The refractive index of air that surrounds the investigated system is $n_0 = 1$. The incident beam of transmission $T_1 = 1$ passes through the film supported on the substrate and the signal measured is T. In a model originally developed by Manaficier et al. [111] and later improved upon by Swanepoel [112], the thickness d of such a film, perpendicular to the incident beam and on the same axis as the detector, can be determined using

$$d = \frac{\Delta i \cdot \lambda_1 \cdot \lambda_2}{2 \cdot (\lambda_2 \cdot n_1 - \lambda_1 \cdot n_2)}, \tag{11}$$

where Δi is the number of fringes between wavelengths at two maxima or minima of interference (λ_1 and λ_2) and n_1 and n_2 are refractive indices at these wavelengths, respectively. This method is valid for measurements carried out in higher wavelength regions, where the film is only weakly absorbing and the substrate is transparent.

Figure 14a shows the spectra obtained for films of DNA made using 0.13, 0.25, and 0.41 mg/cm^2. The interference fringes seen in the transmission spectrum indicate that the film thickness is uniform over the film. If the thickness of the film was tapered or not uniform, these fringes would not be observed as all interference effects destroyed. The thickness of each of the films was calculated using equation (11). Using these values, the volume of the samples can be easily obtained. The average volume over the nine measurements for each mass of DNA is calculated. The inset in Figure 14b shows the final results as a function of DNA mass obtained for all of the DNA films. It was clear that there is a linear relationship between the mass and volume for samples containing between 0.4 and 1.2 mg of DNA spread over the surface of the substrate (Fig. 14b), which results in films of thickness between approximately 1 and 3 μm. To obtain a value for the density of the DNA films, ρ, linear fitting was only performed over this range. A value of the density of CT DNA films was obtained using a least-squares method with weighting to yield

$$\rho = 1.41 \pm 0.03 \text{ g/cm}^3. \tag{12}$$

As expected, the new value was lower than most of those previously reported in the literature for CT DNA

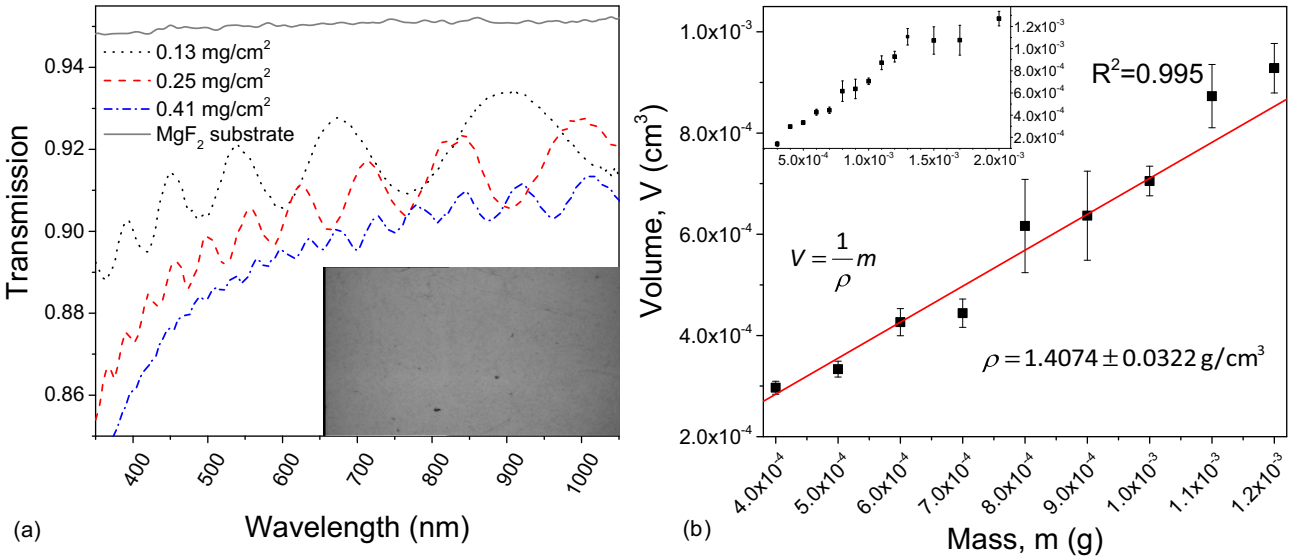

Fig. 14. a) Interference fringes in transmission spectra for calf thymus DNA films of 0.13, 0.25, and 0.41 mg/cm^2, together with transmission measured for the MgF_2 substrate used in the experiments; the inset shows a photograph of the surface of a 0.41 mg/cm^2 film taken on a 40× zoom with an optical microscope; (b) relationship between the mass of CT DNA deposited over the whole surface of MgF_2 substrates and the calculated volume of the sample, fitted with a weighted least-squares method. The inset in b) shows the data points over the whole range investigated [102].

(see Tab. 1 for a comparison with other values reported) and consistent with the conclusions of the previous studies conducted for DNA films [83,84]. The only other result, which is consistent with that presented here was obtained by Inagaki et al. [89], who also used an interferometric method and their value of 1.35 g/cm^3 is in a good agreement (within the experimental error). With all other methods the obtained values of density are higher by approximately 20%. Therefore, by producing films from a wide range of DNA masses it is possible to find a range, in which film formation is uniform and where the thickness increases linearly with the amount of sample. The saturation effect, seen in Figure 14b insert, for DNA masses higher than 1.2 mg per sample can be attributed to reaching a critical value for a film, where the large mass of the material starts compressing its structure.

A newly obtained value of DNA film density proved already to be useful, among others, in the investigations of the DNA-based nanoelectronics [113] and biosensors [114] or in refinement of the outcomes of the theoretical modelling [115].

3 Summary

Although the involvement in the cancer-related research by the AMP community have increased significantly over the past decade, still more input from this community is required. The works reviewed in this paper have shown that better understanding and improvement of experimental methods is needed.

Using an alternative method for SSBs quantification, it was shown that the formation of one DSB in a DNA molecule in an aqueous solution upon VUV irradiation and subsequent hydroxyl radical attack appears to be due to two independent SSBs being formed within approximately 43 bp rather than as a result of a single event. Due to cluster damage that takes place when the damaging agent is hydroxyl radical, the larger value is plausible and when considering any fixed values the experimental conditions have to be kept in mind. Also, it was demonstrated that SSB damage induced upon VUV irradiation has to date been significantly underestimated in radiotherapy models, which provided an explanation for the discrepancies obtained between theoretical and experimental data [116]. Such high levels of damage obtained upon high-dose radiation will be difficult to repair and might interfere with cell cycle progression, at which point cells undergo programmed cell death [117]. All the above allows to conclude that although AGE is popular, easy and inexpensive method, it should not be used for SSBs quantification. Moreover, in order to retrieve as much information as possible from the experimental results, a choice of appropriate theoretical model is required. Revisiting the DNA damage models derived in the past, gave the conditions, for which they are valid and thus ease the choice of appropriate approach [118]. From the above discussion it is clear that choice is heavily dependent on the severity of damage caused by the particles of interest.

It was also shown that far-going assumptions on the film formation may provide a possible explanation of the variations observed in the irradiation experiments and highlight the difficulty in preparing a well-characterised DNA surface, from which quantitative information on irradiation cross sections can be derived. Now it is obvious that the films are not as uniform as assumed and their morphology strongly depends on the preparation conditions. It was also shown that the film is formed as a 3D

network rather than as a multilayer structure and in order to obtain film of a uniform structure additional protocols must be employed. It was also shown that commonly used freeze-drying technique gives by far the worst quality films in terms of their uniformity and surface coverage. Another point that arose was connected to sustainability of the starting material under vacuum conditions. It was shown that plasmid DNA does not stay in its supercoiled form under vacuum conditions and some stabilisers must be added in order to be able to perform any kind of further experiments. Still, more investigations are required in order to establish possible influence of the stabilisers on the experimental outcomes.

Moreover, realising that the density of the dry DNA film is lower indicates that the optical constants for DNA should be recalculated, which were previously obtained assuming a higher DNA concentration in films. The mass per square centimetre quantities used for determining density of dry DNA films are similar to those often used in irradiation studies [57], therefore the lower value should be used in future studies. Furthermore, since it was shown that there is a strong dependence of the sample composition on DNA film formation and thus on its density, interferometric method will be important in characterizing particle interactions with DNA films and the dose dependence [119]. The result presented here also indicates that depending on the film preparation method, i.e. drying conditions and stabilisers used, the value of the density of the film will vary.

M.A.Ś. would like to thank Prof. Nigel J. Mason for his helpful comments on this text. The author also acknowledges the visiting fellow position in the Molecular Physics Group, Open University.

References

1. J. Ferlay, E. Steliarova-Foucher, J. Lortet-Tieulent, S. Rosso, J.W.W. Coebergh, H. Comber, D. Forman, F. Bray, Eur. J. Cancer **49**, 1374 (2013)
2. K. Kobayashi, H. Frohlich, N. Usami, K. Takakura, C. Le Sech, Radiation Research **157**, 32 (2002)
3. M. Rezaee, E. Alizadeh, D. Hunting, L. Sanche, Bioinorg. Chem. Appl. **2012** (2012) 923914
4. M. Rezaee, P. Cloutier, A.D. Bass, M. Michaud, D.J. Hunting, L. Sanche, Phys. Rev. E Stat. Nonlin. Soft Matter Phys. **86**, 031913 (2012)
5. K. Tanzer, A. Pelc, S.E. Huber, M.A. Śmiałek, P. Scheier, M. Probst, S. Denifl, International Journal of Mass Spectrometry **365–366**, 152 (2014), Special issue: Tilmann Merk
6. M.A. Śmiałek, S. Ptasińska, J. Gow, C.D. Pieve, N.J. Mason, Eur. Phys. J. D **68**, 85 (2014)
7. M.A. Śmiałek, S. Ptasińska, J. Gow, S.V. Hoffmann, N.J. Mason, Eur. Phys. J. D **69**, 121 (2015)
8. S.E. Huber, M.A. Śmiałek, K. Tanzer, S. Denifl, J. Chem. Phys. **144**, 224309 (2016)
9. T. Schlathölter, P. Eustache, E. Porcel, D. Salado, L. Stefancikova, O. Tillement, F. Lux, P. Mowat, A.K. Biegun, M.J. van Goethem, H. Remita, S. Lacombe, Inter. J. Nanomedicine **11**, 1549 (2016)
10. R. Schürmann, I. Bald, J. Phys. Chem. C **120**, 3001 (2016)
11. A. Keller, I. Bald, A. Rotaru, E. Cauat, K.V. Gothelf, F. Besenbacher, ACS Nano **6**, 4392 (2012)
12. M.C. Bacchus-Montabonel, M. Łabuda, Y.S. Tergiman, J.E. Sienkiewicz, Phys. Rev. A **72**, 052706 (2005)
13. S. Ptasińska, S. Denifl, P. Scheier, E. Illenberger, T.D. Märk, Angewandte Chemie International Edition **44**, 6941 (2005)
14. I. Baccarelli, I. Bald, F.A. Gianturco, E. Illenberger, J. Kopyra, Phys. Rep. **508**, 1 (2011)
15. M.A. Śmiałek, E. Szymańska, M. MacDonald, L. Zuin, N.J. Mason, Eur. Phys. J.: Special Topics **222**, 2361 (2013)
16. M.A. Śmiałek, M. Labuda, J. Guthmuller, M.J. Hubin-Franskin, J. Delwiche, D. Duflot, N.J. Mason, S.V. Hoffmann, N.C. Jones, P. Limao-Vieira, J. Chem. Phys. **141**, 104311 (2014)
17. I. Bald, E. Illenberger, J. Kopyra, in *Reference Module in Chemistry, Molecular Sciences and Chemical Engineering* (Elsevier, 2014), ISBN 978-0-12-409547-2
18. M. Śmiałek, M. MacDonald, S. Ptasińska, L. Zuin, N. Mason, Eur. Phys. J. D **70**, 42 (2016)
19. C.A. Thomas, P.A. Doty, J. Am. Chem. Soc. **109**, 1854 (1956)
20. D. Freifelder, B. Trumbo, Biopolymers **7**, 681 (1969)
21. G.P. Van Der Schans, Int. J. Rad. Biol. Related Studies in Physics, Chemistry, and Medicine **33**, 105 (1978)
22. W.A. Bernhard, Free Radical Research Communications **6**, 93 (1989)
23. W.A. Bernhard, J. Barnes, K.R. Mercer, N. Mroczka, Radia. Res. **140**, 199 (1994)
24. M.D. Sevilla, C.V. Paemel, C. Nichols, J. Phys. Chem. **76**, 3571 (1972)
25. S.G. Swarts, M.D. Sevilla, Radia. Res. **112**, 21 (1987)
26. W. Wang, M. Sevilla, Radia. Res. **138**, 9 (1994)
27. M.D. Sevilla, D. Becker, in *Electron Spin Resonance*, edited by N.M. Atherton, M.J. Davies, B.C. Gilbert (The Royal Society of Chemistry, 1994), Vol. 14, pp. 130–165, ISBN 978-0-85186-921-6
28. D. Becker, M.D. Sevilla, in *Electron Paramagnetic Resonance*, edited by N.M. Atherton, M.J. Davies, B.C. Gilbert (The Royal Society of Chemistry, 1998), Vol. 16, pp. 79–115, ISBN 978-0-85404-305-7
29. D. Charlton, H. Nikjoo, J. Humm, Int. J. Rad. Biol. **56**, 1 (1989)
30. D.T. Goodhead, Int. J. Rad. Biol. **65**, 7 (1994)
31. J.A. LaVerne, S.M. Pimblott, Radia. Res. **141**, 208 (1995)
32. M. Inokuti, *Atomic and Molecular Data for Radiotherapy and Radiation Research* (International Atomic Energy Agency, Vienna, 1995)
33. V. Cobut, Y. Frongillo, J. Patau, T. Goulet, M. Fraser, J. Jay-Gerin, Radiation Physics and Chemistry **51**, 229 (1998)
34. E. Alizadeh, A.G. Sanz, G. García, L. Sanche, J. Phys. Chem. lett. **4**, 820 (2013)
35. B. Boudaïffa, P. Cloutier, D. Hunting, M. Huels, L. Sanche, Science **287**, 1658 (2000)
36. H. Abdoul-Carime, L. Sanche, Int. J. Rad. Biol. **78**, 89 (2002)

37. Z. Cai, P. Cloutier, D. Hunting, L. Sanche, J. Phys. Chem. B **109**, 4796 (2005)
38. S. Ptasińska, S. Denifl, V. Grill, T.D. Märk, E. Illenberger, P. Scheier, Phys. Rev. Lett. **95**, 093201 (2005)
39. S. Denifl, S. Ptasiska, M. Probst, J. Hruák, P. Scheier, T.D. Mrk, J. Phys. Chem. A **108**, 6562 (2004)
40. S. Feil, K. Gluch, S. Matt-Leubner, P. Scheier, J. Limtrakul, M. Probst, H. Deutsch, K. Becker, A. Stamatovic, T.D. Mrk, J. Phys. B: Atom., Molec. Opt. Phys. **37**, 3013 (2004)
41. S. Denifl, S. Ptasiska, G. Hanel, B. Gstir, M. Probst, P. Scheier, T.D. Mrk, J. Chem. Phys. **120**, 6557 (2004)
42. S. Denifl, H.D. Flosadóttir, A. Edtbauer, O. Ingólfsson, T.D. Märk, P. Scheier, Eur. Phys. J. D **60**, 37 (2010)
43. I. Bald, J. Kopyra, E. Illenberger, Angewandte Chemie International Edition **45**, 4851 (2006)
44. R. Abouaf, J. Pommier, H. Dunet, International Journal of Mass Spectrometry **226**, 397 (2003)
45. S. Gohlke, H. Abdoul-Carime, E. Illenberger, Chem. Phys. Lett. **380**, 595 (2003)
46. H. Abdoul-Carime, S. Gohlke, E. Fischbach, J. Scheike, E. Illenberger, Chem. Phys. Lett. **387**, 267 (2004)
47. M.A. Huels, L. Parenteau, L. Sanche, J. Phys. Chem. B **108**, 16303 (2004)
48. L. Sanche, Eur. Phys. J. D – Atom. Molec. Opti. Plasma Phys. **35**, 367 (2005)
49. E. Alizadeh, L. Sanche, Chem. Rev. **112**, 5578 (2012), pMID: 22724633
50. Z. Deng, I. Bald, E. Illenberger, M.A. Huels, Phys. Rev. Lett. **95**, 153201 (2005)
51. L. Sanche, Mass Spectrometry Reviews **21**, 349 (2002)
52. I.A. Solov'yov, A.V. Yakubovich, P.V. Nikolaev, I. Volkovets, A.V. Solov'yov, J. Comput. Chem. **33**, 2412 (2012)
53. M.A. Śmiałek, J. Phys.: Conf. Ser. **373**, 012013 (2012)
54. J. Van Touw, J. Verberne, J. Retèl, H. Loman, International Journal of Radiation Biology and Related Studies in Physics, Chemistry and Medicine **48**, 567 (1985)
55. M.A. Śmiałek, S.A. Moore, N.J. Mason, D.E.G. Shuker, Radia. Res. **172**, 529 (2009)
56. M.A. Siddiqi, E. Bothe, Radiat. Res. **112**, 449 (1987)
57. B. Boudaïffa, P. Cloutier, D. Hunting, M.A. Huels, L. Sanche, Radia. Res. **157**, 227 (2002)
58. R. Cowan, C.M. Collis, G.W. Grigg, Journal of Theoretical Biology **127**, 229 (1987)
59. W.R. Holley, A. Chatterjee, Radiat. Res. **145**, 188 (1996)
60. A. Deppman, J.O. Echeimberg, A.N. Gouveia, J.D.T. Arruda-neto, Braz. J. Phys. **34**, 958 (2004)
61. E. Surdutovich, O.I. Obolensky, E. Scifoni, I. Pshenichnov, I. Mishustin, A.V. Solov'Yov, W. Greiner, Eur. Phys. J. D **51**, 63 (2009)
62. E. Scifoni, E. Surdutovich, A.V. Solov'Yov, Phys. Rev. E – Statistical, Nonlinear, and Soft Matter Physics **81**, 021901 (2010)
63. E. Surdutovich, E. Scifoni, A.V. Solov'yov, Mutation Research – Reviews in Mutation Research **704**, 206 (2010)
64. E. Surdutovich, A.V. Solovyov, Eur. Phys. J. D **68**, 353 (2014)
65. T. Ito, M. Saito, T. Taniguchi, Photochem. Photobiol. **46**, 979 (1987)
66. W. Sontag, H. Dertinger, International Journal of Radiation Biology and Related Studies in Physics, Chemistry, and Medicine **27**, 543 (1975)
67. M.A. Śmiałek, S.V. Hoffman, M. Folkard, K.M. Prise, D.E.G. Shuker, N.S.J. Braithwaite, N.J. Mason, J. Phys.: Conf. Ser. **101**, 012020 (2008)
68. M. Folkard, K.M. Prise, B. Brocklehurst, B.D. Michael, J. Phys. B: Atom. Molec. Opti. Phys. **32**, 2753 (1999)
69. J. Chen, K. Jin, M. Chen, W. Pei, K. Kawaguchi, D.A. Greenberg, R.P. Simon, J. Neurosci. **69**, 232 (1997)
70. A. Bopp, S. Carpy, B. Burkart, U. Hagen, Biochimica et Biophysica Acta (BBA) – Nucleic Acids and Protein Synthesis **294**, 47 (1973)
71. Q. Bao, Y. Chen, Y. Zheng, L. Sanche, J. Phys. Chem. C, Nanomaterials and Interfaces **118**, 15516 (2014)
72. J. Ward, G. Jones, J. Milligan (INVITED), Radiation Protection Dosimetry **52**, 271 (1994)
73. A. Keller, J. Rackwitz, E. Caut, J. Livin, T. Krzdrfer, A. Rotaru, K.V. Gothelf, F. Besenbacher, I. Bald, Sci. Rep. **4**, 7391 (2014)
74. S. Vogel, J. Rackwitz, R. Schrman, J. Prinz, A.R. Milosavljevi, M. Rfrgiers, A. Giuliani, I. Bald, J. Phys. Chem. Lett. **6**, 4589 (2015)
75. S.V.K. Kumar, T. Pota, D. Peri, A.D. Dongre, B.J. Rao, J. Chem. Phys. **137**, 045101 (2012)
76. Y. Chen, A. Aleksandrov, T.M. Orlando, Int. J. Mass Spectrometry **277**, 314 (2008)
77. T.M. Orlando, D. Oh, Y. Chen, A.B. Aleksandrov, J. Chem. Phys. **128**, 195102 (2008)
78. K. Dose, A. Bieger-Dose, O. Kerz, M. Gill, Origins of Life and Evolution of the Biosphere **21**, 177 (1991)
79. J. Wyer, K. Butterworth, D. Hirst, C. Latimer, E. Montenegro, M. Shah, F. Currell, Phys. Med. Biol. **54**, 4705 (2009)
80. M. Folkard, K.M. Prise, B. Vojnovic, S. Davies, M.J. Roper, B.D. Michael, Int. J. Rad. Biol. **64**, 651 (1993)
81. S.V.K. Kumar, M. Murali, P. Kushwaha, Eur. Phys. J. D **69**, 204 (2015)
82. M. Folkard, K.M. Prise, B. Vojnovic, B. Brocklehurst, B.D. Michael, Int. J. Rad. Biol. **76**, 763 (2000)
83. M.A. Śmiałek, N.C. Jones, R. Balog, N.J. Mason, D. Field, Eur. Phys. J. D **62**, 197 (2011)
84. M.A. Śmiałek, R. Balog, N.C. Jones, D. Field, N.J. Mason, Eur. Phys. J. D **60**, 31 (2010)
85. M.A. Huels, B. Boudaiffa, P. Cloutier, D. Hunting, L. Sanche, J. Am. Chem. Soc. **125**, 4467 (2003)
86. O. Boulanouar, A. Khatyr, G. Herlem, F. Palmino, L. Sanche, M. Fromm, J. Phys. Chem. C **115**, 21291 (2011)
87. M. Fromm, O. Boulanouar, Radiat. Phys. Chem. **128**, 43 (2016)
88. J. Liu, X. Yao, P. Cloutier, Y. Zheng, L. Sanche, J. Phys. Chem. C **120**, 487 (2016)
89. T. Inagaki, R. Hamm, E. Arakawa, J. Chem. Phys. **61**, 4246 (1974)
90. A. Samoc, A. Miniewicz, M. Samoc, J.G. Grote, J. Appl. Polym. Sci. **105**, 236 (2007)
91. I. Abril, R. Garcia-Molina, C.D. Denton, I. Kyriakou, D. Emfietzoglou, Rad. Res. **175**, 247 (2011)
92. C.J. Tung, W.T. Chan, T.C. Chao, Y.H. Tu, C.M. Kwei, Nucl. Instrum. Meth. A **580**, 598 (2007)
93. Z. Tan, Y. Xia, M. Zhao, X. Liu, Nucl. Instrum. Meth. B **248**, 1 (2006)

94. J.A. LaVerne, S.M. Pimblott, Radia. Res. **141**, 208 (1995)
95. J.C. Ashley, M.W. Williams, Radia. Res. **81**, 364 (1980)
96. K.M. Prise, M. Folkard, B.D. Michael, B. Vojnovic, B. Brocklehurst, A. Hopkirk, I.H. Munro, Int. J. Rad. Biol. **76**, 881 (2000)
97. Z. Tan, Y. Xia, M. Zhao, X. Liu, F. Li, B. Huang, Y. Ji, Nucl. Instrum. Meth. B **222**, 27 (2004)
98. K. Hieda, Y. Hayakawa, A. Ito, K. Kobayashi, T. Ito, Photochem. Photobiol. **44**, 379 (1986)
99. W.T. Astbury, X-ray studies of nucleic acids, Symp. Soc. Exp. Biol. **1**, 66 (1947)
100. R.E. Franklin, R.G. Gosling, Acta Crystallographica **6**, 678 (1953)
101. T. Weidlich, S.M. Lindsay, A. Rupprecht, Biopolymers **26**, 439 (1987)
102. M.A. Śmiałek, N.C. Jones, S.V. Hoffmann, N.J. Mason, Phys. Rev. E **87**, 60701 (2013)
103. H. Votavova, J. Sponar, Nucleic Acids Res. **2**, 431 (1975)
104. J.P. Thiery, G. Macaya, G. Bernardi, J. Molec. Biol. **108**, 219 (1976)
105. G. Macaya, J. Cortadas, G. Bernardi, Eur. J. Biochem. **84**, 179 (1978)
106. J. Filipski, J.P. Thiery, G. Bernardi, J. Molec. Biol. **80**, 177 (1973)
107. S.N. Cohen, A.C. Chang, H.W. Boyer, R.B. Helling, Proc. Natl. Acad. Sci. (USA) **70**, 3240 (1973)
108. F. Gautier, H. Bünemann, L. Grotjahn, Eur. J. Biochem. / FEBS **80**, 175 (1977)
109. J.E. Hearst, J. Vinograd, Proc. Natl. Acad. Sci. (USA) **47**, 1005 (1961)
110. J. Vinograd, R. Greenwald, J.E. Hearst, Biopolymers **3**, 109 (1965)
111. C.J. Manifacier, J. Gasiot, J.P. Fillard, J. Phys. E: Sci. Instrum. **9**, 1002 (1976)
112. R. Swanepoel, J. Phys. E: Sci. Instrum. **16**, 1214 (1983)
113. Z. Xu, X. Wang, H. Xie, Polymer **55**, 6373 (2014)
114. K. Fu, B.G. Willis, Sensors and Actuators B: Chemical **220**, 1023 (2015)
115. C. Champion, M.A. Quinto, J.M. Monti, M.E. Galassi, P.F. Weck, O.A. Fojón, J. Hanssen, R.D. Rivarola, Phys. Med. Biol. **60**, 7805 (2015)
116. H. Rabus, H. Nettelbeck, Radiation Measurements **46**, 1522 (2011)
117. M. Chen, Q. Huang, W. Xu, C. She, Z.G. Xie, Y.T. Mao, Q.R. Dong, M. Ling, PLoS ONE (2014)
118. K. Pachnerová Brabcová, L. Sihver, N. Yasuda, Y. Matuo, V. Štěpán, M. Davidkova, Radiation and Environmental Biophysics **53**, 705 (2014)
119. L. Vyšín, K. Pachnerová Brabcová, V. Štěpán, P. Moretto-Capelle, B. Bugler, G. Legube, P. Cafarelli, R. Casta, J.P. Champeaux, M. Sence et al., Radiation and Environmental Biophysics **54**, 343 (2015)